The Role of Plasticity in Bimaterial Fracture with Ductile Interlayers

N.I. TYMIAK, A.A. VOLINSKY, M.D. KRIESE, S.A. DOWNS, and W.W. GERBERICH

Evaluation of the plasticity effects in fracture along ductile/brittle interfaces requires appropriate models for plastic dissipation in a ductile component. For thin ductile films, constitutive properties appropriate to the small volumes involved are essential for adequate modeling. Here, yield stress is of primary importance. With nanoindentation, one can obtain both a large strain flow stress as well as the far field yield stress representing the small strain elastic-plastic boundary. Using these to estimate an appropriate plastic strain energy density, the crack tip plastic energy dissipation rates associated with the interfacial crack extension can be estimated for a ductile film. With the preceding analysis, plasticity effects on the interfacial toughness have been evaluated for external measures of strain energy release rates as obtained from indentation tests using the axisymmetric bilayer theory. Comparison involved RF sputtered 200- to 2000-nm-thick Cu interlayers between oxidized silicon and sputtered tungsten. Experimental values for the Cu/SiO_2 interface increased with Cu film thickness from 1 to 15 J/m^2. This was in qualitative agreement with the theoretical predictions for plastic energy dissipation rates. In contrast, first-order estimates suggest that the observed interfacial toughness increases cannot be attributed to either mode mixity effects or increased intrinsic interfacial fracture energies. As such, crack tip plasticity is identified as the dominant mechanism for increasing interfacial toughness.

I. INTRODUCTION

ADHESION of thin metallic films is one of the most important reliability issues in microelectronics. A device may fail due to poor adhesion even if the material of the film itself satisfies the design criteria. Numerous mechanisms have been identified as fundamental to the adhesion of thin films and debonding of metal/ceramic interfaces. Interfacial fracture energy, Γ_0, an energy necessary to create free surfaces from a bonded interface, is determined primarily by the true interfacial surface energy, a quantity commonly measured by the contact angle technique.[1] A variety of microstructural factors in the fracture process zone would also affect Γ_0. These include mechanical interlocking, phase intermixing, and/or existing defects along an interface. Interfacial fracture energy may be evaluated by delaminating a thin film from the substrate. However, before a thin metallic film debonds from the substrate, it usually experiences plastic deformation. It is difficult to extract the interfacial fracture energy from the total energy measured. What is measured is the practical work of adhesion. In terms of the critical strain energy release rate, G_{crit}, *i.e.*, elastic energy released per unit of fracture area,

$$G_{crit} = \Gamma_0 + \Gamma_p + \text{other forms of dissipation} \quad [1]$$

Here, Γ_p is the crack tip plastic energy dissipation rate. The stronger the interface is (higher Γ_0) the more energy is dissipated through plastic deformation. Compared with the other dissipation terms, Γ_p is prevalent except, possibly, for very thin films and/or high interfacial roughness where frictional losses may be significant.[2] Plastic energy dissipation is suggested as a dominant mechanism involved in the increase of the experimentally measured interfacial fracture toughness with the film thickness increase.[3,4] For a Cu/SiO_2 interface, this trend was observed for adhesion determined with the different methods.[4] However, there is a possibility that intrinsic interfacial strength increases with the increasing film thickness as a consequence of differences in deposition/processing involved in obtaining different film thicknesses. Also, with increasing film thickness, mode mixity may change. The experimentally measured practical work of adhesion generally increases with the crack tip becoming more heavily under mode II conditions.[5] Increasing frictional[2] and/or plasticity[6] losses are suggested as the most probable mechanisms. Taking into account the previous considerations, evaluation of the plasticity effects in the interfacial toughness elevation with increasing film thickness would require the following:

(1) establishment of the theoretical dependence between film thickness and plastic energy dissipation;
(2) experimental evaluation of thickness effects for a broad range of Cu interlayer thicknesses with comparison to theoretical predictions;
(3) extraction of a true characteristic of the interfacial strength from the experimental data;
(4) assessment of mode mixity as a function of film thickness; and
(5) evaluation of the constitutive properties of the nanostructured thin Cu interlayers required for the analysis of the plasticity effects.

Mechanical properties of nanostructured materials have been shown to be highly dependent both on the synthesis

N.I. TYMIAK and A.A. VOLINSKY, Graduate Students, and W.W. GERBERICH, Professor, are with the Department of Chemical Engineering and Materials Science, University of Minnesota, Minneapolis, MN 55455. M.D. KRIESE, Research Scientist, is with Osmic Inc., Troy, MI 48084. S.A. DOWNS, Applications Scientist, is with Hysitron Inc., Minneapolis, MN 55439.

This article is based on a presentation made in the Symposium "Mechanisms and Mechanics of Composites Fracture" held October 11–15, 1998, at the TMS Fall Meeting in Rosemont, Illinois, under the auspices of the TMS-SMD/ASM-MSCTS Composite Materials Committee.

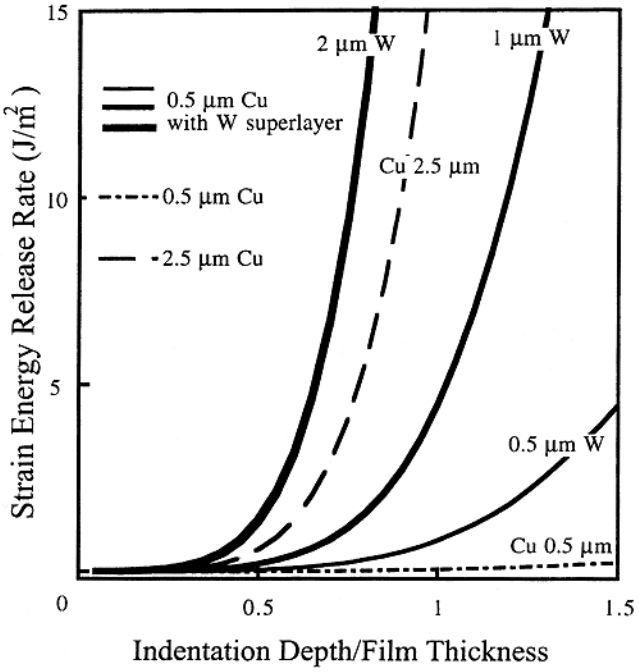

Fig. 1—Effects of W superlayer on the energy available for crack extension.

method and the way properties have been evaluated.[7,8] From the current literature, it did not appear that existing correlations between mechanical behavior of nanostructured Cu *vs* grain size and/or film thickness were directly applicable.

II. THEORETICAL

A. *Interfacial Energies by Superlayer Indentation*

Indentation-based adhesion testing provides a simple and reliable experimental procedure supported by rigorous theoretical analysis.[9,10,11] However, this method is not directly applicable to ductile strongly adherent films. In this case, extensive plastic deformation occurs before strain energy sufficient for the delamination can be accumulated. Difficulties with delamination initiation can be overcome by depositing a superlayer over the film of interest.[4] The presence of the superlayer provides an additional driving force for delamination, as shown in Figure 1. Also, a superlayer would impose constraint on the plastic flow in the underlying film. This can result in additional normal stress at the interfacial crack tip.[12] Bagchi *et al.*[4] used bimaterial lines with previously induced interfacial cracks. Compared to the previous mention and approach, an indentation-based bilayer method developed by Kriese *et al.*[13,14] has an advantage of being a very simple experimental procedure combined with the ease of sample preparation. The method relies on the extension of a single layer solution[11] for the case of a bimaterial film. During a typical test, load is increased to a prescribed peak value, held at this value, and then decreased back to zero. Under increasing indentation load, a circular interfacial crack nucleates and extends. Buckling under indentation loading (double buckling) is possible providing stress in a delaminated portion of a film exceeds a critical value. After load removal, a delaminated film buckles (single buckling) if stress in a delaminated film is higher than an appropriate critical value. Following a single buckling, further crack

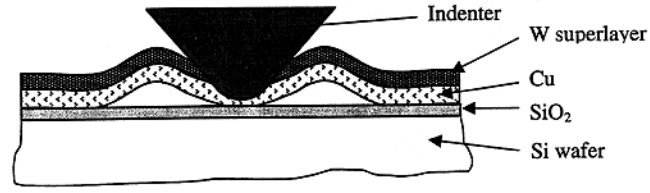

Fig. 2—Schematic of bilayer indentation.

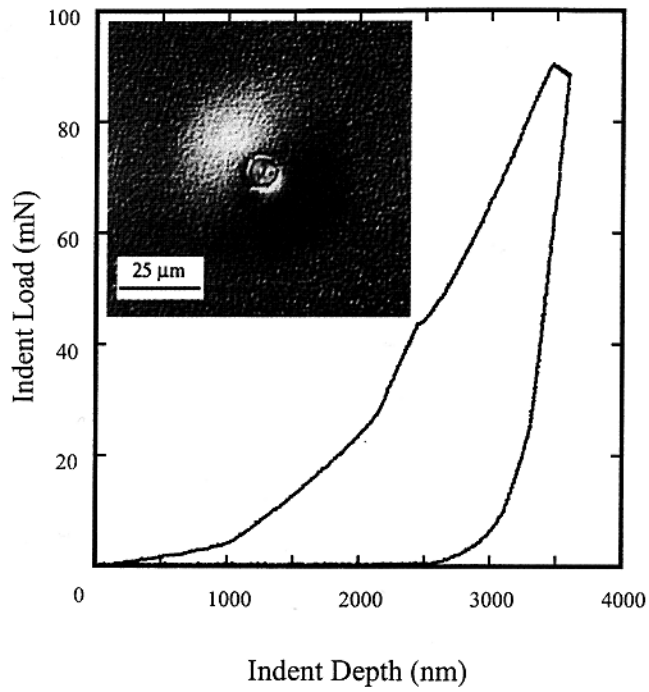

Fig. 3—Indentation induced blister and corresponding load-displacement curve.

extension is possible. For a given delamination radius, the critical stress for double buckling is always higher than that for single buckling. A schematic of the processes occurring during bilayer indentation is shown in Figure 2. The figure corresponds to double buckling. An example of indentation induced blister alongside with the corresponding indentation curve is shown in Figure 3. Critical strain energy release rate, G_{crit}, is defined as a function of the following parameters:[14,15] E_i, Young's moduli; ν_i, Poisson's ratios; σ_{Ri}, residual stresses; R, delamination radius; and $\sigma_{indentation}$, an effective indentation induced stress. Here, $i = 1, 2$ with 1 and 2 corresponding to a film and a superlayer, respectively. Indentation induced stress is evaluated from the volume of material displaced during indentation, V_0 (indentation volume). The indentation volume can be determined based either on the recorded indenter penetration depth or from direct measurements of indentation induced delaminations. For the latter determinations, either AFM or profilometry may be used. The strain energy release rate is assigned to be equal to nonbuckled, single buckled, or double buckled conditions. For a given test, it is assumed that $G = G_{nonbuckled}$ if stress does not exceed any of the single or double buckling critical stresses, or if $G_{nonbuckled} > G_{single\ buckled}$, and the stress is not sufficient for double buckling; $G = G_{double\ buckled}$ if double buckling stress is reached, and $G_{double\ buckling} > G_{single\ buckling}$; otherwise, $G = G_{single\ buckled}$.

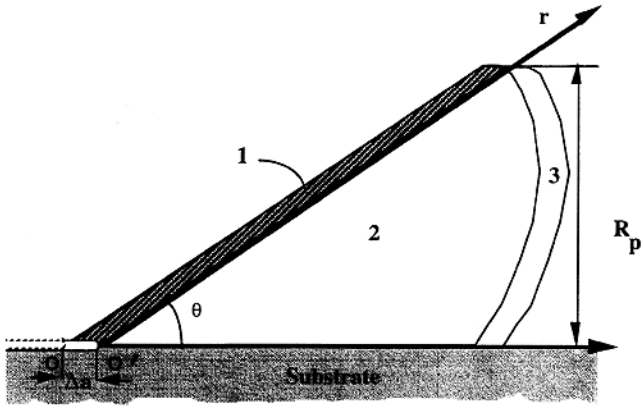

Fig. 4—Plastic zone translation associated with the crack tip advance from O to O′. Total plastic energy dissipation increment associated with the preceding crack advance is equal to the plastic energy dissipation in the shaded portion.

B. *Upper Bound Plastic Energy Dissipation Model*

A model considers an elastic-plastic film sandwiched between an elastic substrate and elastic superlayer. Evaluation of plastic energy dissipation associated with the interfacial crack extension requires knowledge of the crack tip plastic zone evolution. In general, an active plastic zone both translates and changes its shape/dimensions during crack growth. A precise formulation of the problem would require determination of an active plastic zone shape and corresponding plastic strain distribution as functions of the crack length. These should be determined with the consideration of both substrate and superlayer effects. A possibility of plastic deformation in the substrate and/or a superlayer should be evaluated as well. In addition, as plastic deformation is affected by hardening, it should ideally be included into modeling. Also, with the extent of plastic deformation dependent on the intrinsic interfacial toughness, Γ_0, this parameter should also enter into model formulation.

The present first-order model assumes the following largely simplified conditions:

(1) elastic–perfectly plastic film (no hardening);
(2) no plastic deformation in either the substrate or a superlayer; and
(3) plastic energy dissipation rate independent of crack length.

Note that (3) implies quasistatic conditions where translation of a plastic zone occurs without change of its shape/dimensions and associated plastic strain redistribution.

Plastic energy dissipation rate, Γ_p, can be determined as follows:

$$\Gamma_p = \lim_{\Delta A \to 0} \frac{\Delta W_p}{\Delta A} \qquad [2]$$

where ΔA and ΔW_p are increments in crack area and plastic strain energy, respectively, with ΔA given by

$$\Delta A = 2\pi a \Delta a \qquad [3]$$

Here, Δa is a crack length increment.

ΔW_p includes the two following contributions, as shown in Figure 4:

(1) plastic deformation of a previously elastic region 3; and
(2) an additional energy dissipation in region 2 that was already plastically deformed prior to a crack advance.

With the above, ΔW_p will be equal to the difference between a total plastic energy dissipated in a "new" plastic zone and plastic energy dissipated in region 2 prior to the crack advance. Since both $\varepsilon_p(r)$ and R_p are assumed the same for new and "old" plastic zones, the difference will be equal to the plastic energy dissipated in strip 1 and may be estimated as follows:

$$\Delta W_p = \bar{\sigma}\,\bar{\varepsilon}_p\,\Delta V_p \qquad [4]$$

Here, ΔV_p is a volume of a strip; $\bar{\sigma} = \sigma_{ys}$, an average stress in the plastic zone; and $\bar{\varepsilon}_p$, an average plastic strain. The plastic strain $\varepsilon_p(R_p, r)$, at the distance r from the crack tip, may be approximated by the following:[16]

$$\varepsilon(R_p, r) = \frac{\sigma_{ys}}{E} \cdot \left(\frac{R_p}{r} - 1\right) \qquad [5]$$

Here, a relation originally derived for mode III is used, with the shear modulus, μ, replaced by E, Young's modulus, and a shear yield stress substituted by a tensile yield stress. In the previous discussion, we follow a procedure suggested by McClintock and Irwin[17] for obtaining the mode I analog from the mode III elastic-plastic solution. In the original approach,[16] R_p denotes a radius of a spherical plastic zone. The FEM analysis for an interfacial crack between a ductile film and elastic substrate[6] suggests a wing-shaped plastic zone, as shown in Figure 4. A characteristic inclination angle θ decreases with the increasing fraction of mode II from 90 deg for a pure mode I condition to approximately 45 deg under equal contributions of modes I and II.[6] Although the presence of a superlayer will introduce additional complexities, a similar trend may be assumed for a present case. Under these conditions, the extent of the plastic zone in the direction perpendicular to the crack plane is restricted to a film thickness. However, it is not excluded that the lateral extent of the plastic zone may eventually exceed film thickness.

For an arbitrary angle θ (Figure 4),

$$\Delta V_p \approx 2\pi a R_p\,\Delta a \qquad [6]$$

With small Δa, plastic strain gradient in the lateral direction can be neglected, and $\bar{\varepsilon}_p$ can be determined as follows:

$$\bar{\varepsilon}_p = \frac{1}{(R_p/\sin\theta) - \Delta} \int_{\Delta}^{R_p/\sin\theta} \varepsilon\,(R_p/\sin\theta, r)\,dr \qquad [7]$$

where Δ is a characteristic cut-off distance from a crack tip. Introduction of a characteristic length parameter removes the singularity of plastic strain at the crack tip.[18] Substituting Eq. [3] into Eq. [7] and integrating yields

$$\bar{\varepsilon}_p = \frac{\sigma_{ys}}{E}\left\{\ln\left[\frac{R_p/\sin\theta}{\Delta}\right] - 1 + \frac{\Delta}{R_p/\sin\theta}\right\} \qquad [8]$$

Based on Eqs. [2] through [4], [6], and [8], the plastic energy dissipation rate can be determined

$$\Gamma_p = \{R_p/\sin\theta\}\,\frac{\sigma_{ys}^2}{E}\left\{\ln\left[\frac{R_p/\sin\theta}{\Delta}\right] - 1 + \frac{\Delta}{R_p/\sin\theta}\right\} \qquad [9]$$

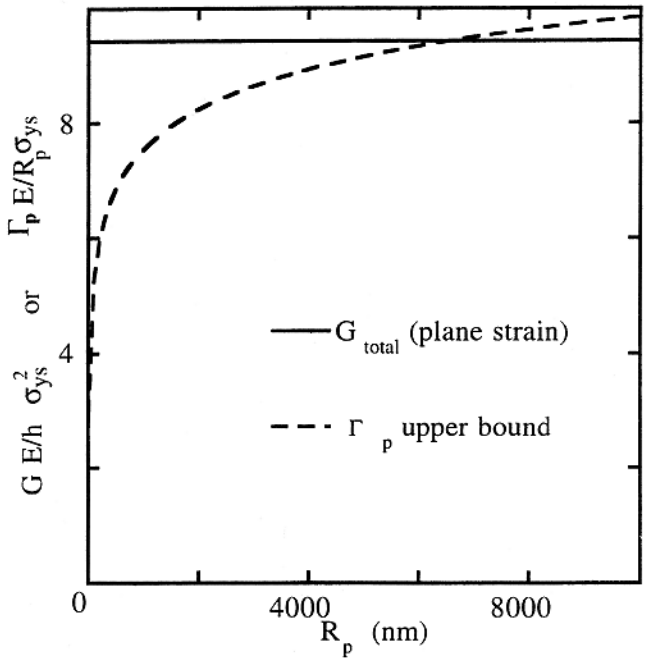

Fig. 5—A comparison between normalized *total* strain energy release rate as given by a small scale yielding plane strain solution and an upper bound solution for plastic energy dissipation rate.

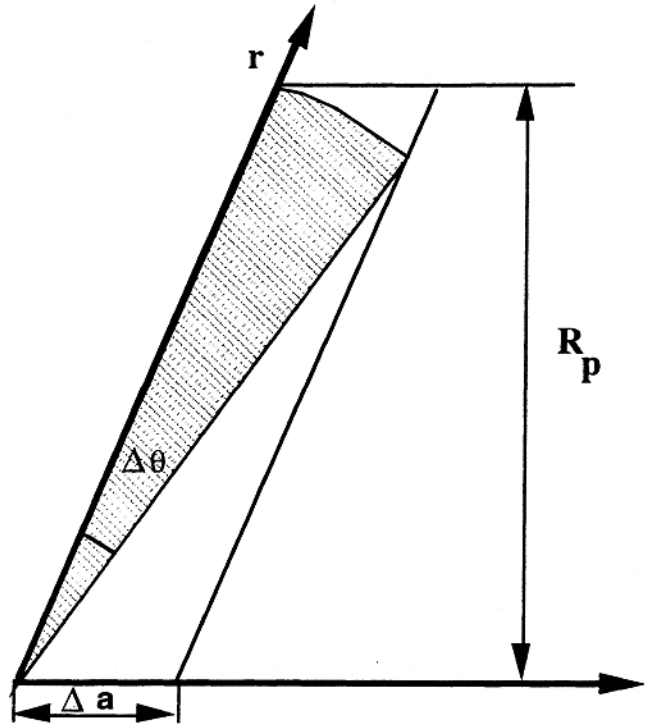

Fig. 6—A lower bound estimate of the average plastic strain. Here, an average over the shaded sector would include only part of plastic strain associated with the crack advance, Δa.

Here, $R_p/\Delta > 1$ and Γ_p increases with an increase in R_p/Δ. Thus, an upper bound for Γ_p would be, at the maximum, R_p, and a minimum, Δ. For parameter Δ, a lower bound would clearly be a burgers vector, **b**. On the other hand, film thickness would be the maximum possible value for R_p. Analysis of the scratch tests[3] on Pt and Ti films suggested that over a range of film thicknesses, the whole thickness of metal was plastically deforming during delamination. Even taking into account the difference in the stress-strain states involved during scratch and indentation, assuming the plastic zone size is equal to the film thickness appears to be a reasonable first-order estimate.

Figure 5 shows the plastic energy dissipation rate as given by Eq. [4] with $\Delta = \mathbf{b} = 0.25$ nm and $\theta = 90$ deg. This upper bound solution is compared to a *total* strain energy release rate, G_{total}, as estimated based on the small scale yielding solution

$$G_{\text{total}} = \frac{3\pi\sigma_{ys}^2 R_p}{E} \qquad [10]$$

Equation [10] is appropriate for plane strain conditions generally accepted for axysymmetric delamination problems.[11,19] Being only a part of the total elastic-plastic strain release rate, the plastic energy disssipation rate from Eq. [9] should not exceed G_{total}. From Figure 5, it is seen that with an increasing R_p, the upper bound solution approaches and eventually exceeds G_{total}. This overestimate of plastic energy dissipation rates results when the plastic zone size reaches a critical value of approximately 6000 nm. For the present study, film thicknesses ranged only up to 2000 nm. Thus, even assuming plastic zones extending through the entire film thickness, Eq. [9], still will be applicable. Note also that with the cut-off distance larger than a burgers vector, applicability of an upper bound solution will be extended to even higher plastic zone radii.

As an alternative to Eq. [7], $\bar{\varepsilon}_p$ may be estimated by taking an average over a sector instead of a strip as shown in Figure 6. This will yield the following:

$$\bar{\varepsilon}_p = \frac{\int_{\Delta\theta}\int_{0}^{R_p/\sin\theta} \varepsilon\, r\, dr\, d\varphi}{\int_{\Delta\theta}\int_{0}^{R_p/\sin\theta} r\, dr\, d\varphi} = \frac{\sigma_{ys}}{E} \qquad [11]$$

Note that an $\bar{\varepsilon}_p$ defined with Eq. [11] is independent of the angle $\Delta\theta$ over which an average is taken. Thus, plastic strain averaged over an entire plastic zone will also be equal to σ_{ys}/E. With $\bar{\varepsilon}_p$ from Eq. [11] combined with Eqs. [2] through [4] and [6], plastic energy dissipation becomes

$$\Gamma_p = \{R_p/\sin\theta\}\,\frac{\sigma_{ys}^2}{E} \qquad [12]$$

Such a procedure eliminates the necessity of introducing a cut-off distance. However, a substantial part of the highly strained near-tip region was not included in $\bar{\varepsilon}_p$, giving an underestimated Γ_p. Thus, Eq. [12] may be regarded as a lower bound estimate for plastic energy dissipation rates for a given plastic zone size.

C. *Bond Strength and Phase Angle Estimate*

Based on the plastic energy dissipation estimates and the critical energy rate balance Eq. [1], an intrinsic interfacial adhesion strength can possibly be evaluated in terms of an interfacial fracture energy, Γ_0. Intrinsic adhesion strength of an interface may also be assessed *via* a characteristic critical

stress parameter based on an appropriate model of the fracture process.

An estimate of the characteristic stress parameter from the experimentally measured values of G can be accomplished by extending an approach suggested by Mao *et al.*[20] for pure mode I conditions. The approach relies on a model of discontinuous interfacial crack growth. According to the model, fracture occurs as normal stress ahead of a blunted crack tip reaches a critical value, σ_b, which is denoted as interfacial bond strength. Following a fracture event, the crack extends until a blunting induced arrest. Crack tip blunting occurs as a consequence of activation of near-tip dislocation sources.[21] The above mechanism is applicable to a relatively weak metal ceramic interfaces as opposed to strong interfaces where fracture involves void nucleation and coalescence. Based on the model of Mao *et al.*, the strain energy release rate corresponding to the onset of fracture can be determined as follows:

$$G_0 = \left(\frac{\pi}{8}\right)\frac{\sigma_b^2 \Delta}{E} \qquad [13]$$

Here, G_0 is the initiation strain energy release rate; $\Delta = N_b$, with N being the number of dislocations involved in the crack blunting; and **b** is the burgers vector. Assuming $N \approx \frac{Hh}{\mu \mathbf{b}}$ [22] with the hardness, $H \approx 3\sigma_{ys}$,[23] and solving for σ_b yields

$$\sigma_b = \sqrt{\frac{8E\mu G}{3\pi h \sigma_{ys}}} \qquad [14]$$

Here, μ is the shear modulus of the film. Applying this equation to the values of G measured from our experiments, we neglect the difference between G_0 and G_s corresponding to crack *initiation* and *propagation* resistance, respectively. It should also be noted that in our case, σ_b is not a tensile bond strength but rather the measure of the strength corresponding to the particular phase angle ψ which is given by

$$\psi = \tan^{-1}\left(\frac{\tau}{\sigma}\right) \qquad [15]$$

Here, σ and τ are normal and tangential stress at some small distance, ρ, from the crack tip. To the first order, the tangential stress component at the interface can estimated with[24]

$$\frac{\tau_r}{p_0} = \frac{1}{\sqrt{18}}\left\{-2(1+\nu)\left[1 - \frac{r}{a}\tan^{-1}\left(\frac{a}{r}\right)\right] + 3\left(\frac{r^2}{a^2}\right)^{-1}\right\} \qquad [16]$$

In this equation,* $p_0 \approx 1.5H$ is the maximum indentation pressure; a = $\sqrt{\delta R}$ is the contact radius; R is the effective tip radius; δ is the penetration depth under maximum load; and r is the distance to the interface. The latter is calculated as $r = h_{Cu} + h_w - \delta_r$, with δ_r being the residual penetration depth and h_{Cu} and h_w copper and tungsten layer thicknesses, respectively. The effective tip radius is defined at $\delta + \delta_b$. Here, δ_b is the tip blunting distance which is 414 nm for a 90 deg cone of a 1-μm tip radius. Equation [16] is applicable for penetration depths not exceeding the bilayer thickness.

Determination of mode mixity corresponding to experimentally measured critical strain energy release rate would require values of normal and tangential stresses as associated with the critical condition. Here, it is assumed that $\sqrt{\sigma^2 + \tau^2} = \sigma_b$ will be appropriate, thus, yielding

$$\psi = \tan^{-1}\left(\frac{\tau}{\sqrt{\sigma_b^2 - \tau^2}}\right) \qquad [17]$$

*Note this provides just a first-order estimate. More precise consideration would be required for the following: elastic constant mismatch for two materials forming an interface; effect of a superlayer; and changes in stress state due to interfacial crack initiation and propagation.

III. EXPERIMENTAL PROCEDURES

A. *Sample Preparation*

The substrates were 10-cm-diameter ⟨100⟩ single-crystal Si wafers. These were oxidized prior to film deposition to produce 3 μm of SiO_2 as described elsewhere.[14] For film deposition, a RF sputtering system was used. A detailed procedure description was published previously.[15] With a DEKTAK surface profiler, film thickness measurements have been made ranging from 200 to 2000 nm. Residual stresses evaluated with the wafer bow technique[14] were 200 to 300 MPa (tensile) and 200 to 300 MPa (compressive) for Cu films and W superlayers, respectively.

B. *Fracture Toughness Determination*

Displacement controlled indentation tests were carried out with the IBM micromechanical tester. An analogous device has been described elsewhere.[25] A conical 90 deg diamond indenter with an approximately 1-μm tip radius has been used to produce a series of indents at different prescribed peak loads. With optical interferometry and profilometry, delamination radii were assessed. Indentation volume computation was based on the unloading curve analysis as detailed elsewhere.[14,15]

C. *Yield Strength and Grain Size Evaluation*

Application of either Eq. [9] or [12] requires yield stress for each film thickness. Prior plastic zone evaluations[3] were partially based upon either an assumption that the yield stress for annealed Ti films was relatively independent of film thickness, or yield strength of nanocrystalline or could be scaled to palladium. For more reliable results, the present study used yield stress either determined on the same films from which the interfacial energies were obtained or at least on the films produced with the same sputtering setup under the same conditions.

Grain size for all film thicknesses was estimated from AFM images. An example of the 500 nm film is shown in Figure 7. For the films thicker than 500 nm, this method becomes less reliable due to increasing surface roughness. Here, TEM and/or FEG SEM measurements would probably be a better choice in this range.

Indentation tests to determine Cu film constitutive properties were carried out with the Hysitron nanoindenter, an AFM attachment that combines nanoindentaton and imaging of a tested area. A conical 90 indenter with approximately a 400-nm tip radius was used. From the load-displacement curves, the Young's modulus and hardness were calculated using the Oliver and Pharr method.[26] Yield stress has been

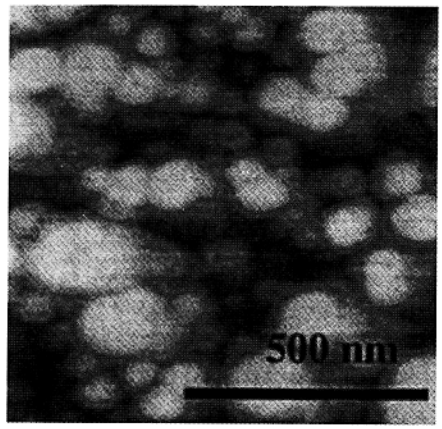

(*a*)

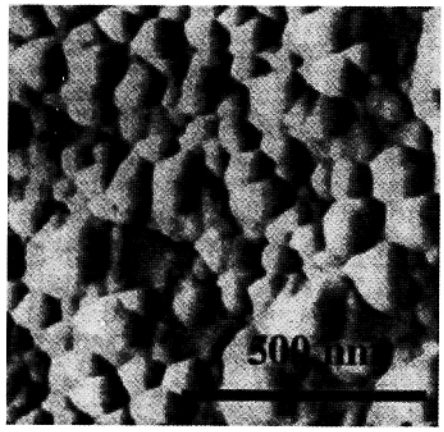

(*b*)

Fig. 7—An AFM image of a 500-nm Cu film: (*a*) height image and (*b*) deflection image.

estimated as 1/3 of hardness values.[23] Only tests at penetration depth sufficient to neglect roughness effects were used for the analysis. For films from 200 to 500 nm, depths exceeding 1/10 of film thicknesses were required.

Substrate effects were apparent, as shown in Figure 8, for 200-nm film where measured hardness increases from 3.3 to 4.6 GPa with the penetration depth increasing from 50 to 130 nm. Correction was accomplished with the Bhattacharya and Nix's method.[27] The hardness ratio $H_{film}/H_{substrate}$ was determined to provide the best fit to the $H_{measured}/H_{substrate}$ *vs* depth/film thickness dependence, as shown in Figure 9. Here, substrate hardness was taken as hardness of thermally grown SiO_2. The $H_{substrate}$ = 8.1 GPa was determined from the indentation into an oxidized Si wafer identical to these used for Cu/W deposition.

IV. RESULTS AND DISCUSSION

A. *Yield Strength Relationship*

Grain sizes estimated with the AFM are presented in Table I. From this table, it is evident that grain size scales with the film thickness are only for up to about 200-nm-thick films. Yield stress *vs* grain size dependence is shown in Figure 10. It appears that the dependence $\sigma_{ys} = \sigma_0 + kd^{-1}$ provides a slightly better fit for the data compared with the Hall–Petch equation $\sigma_{ys} = \sigma_0 + kd^{-1/2}$. A similar trend has

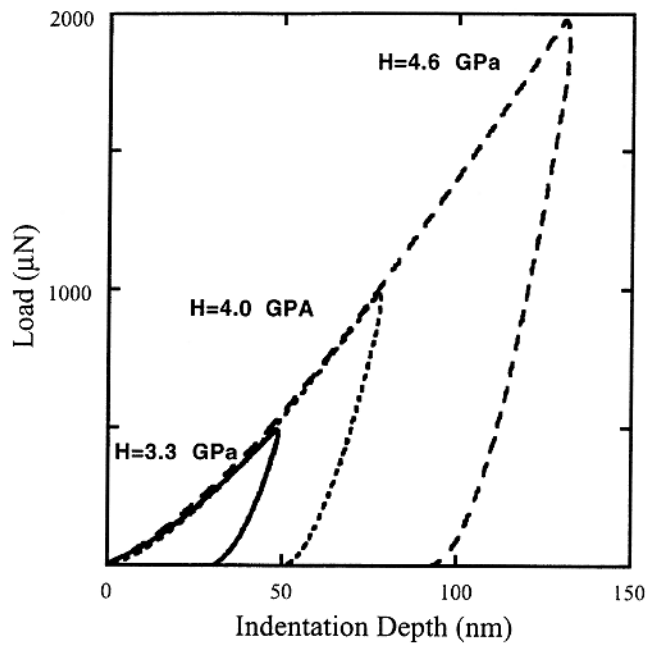

Fig. 8—Indentation curves for a 200-nm Cu film. Substrate effect is apparent from hardness values increasing with penetration depth.

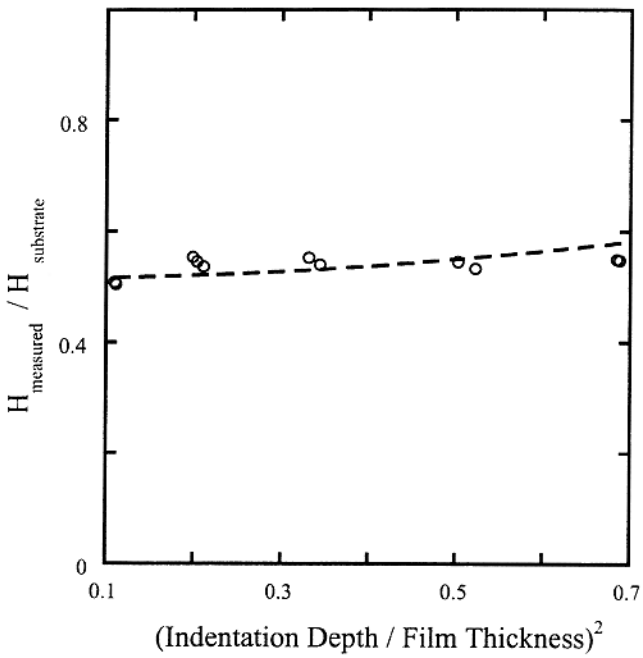

Fig. 9—Substrate effect correction. Here, H_f, the Cu film hardness, is determined from the best fit to the experimental data.

Table I. Cu Film and Cu/SiO_2 Interfacial Fracture Characteristics

h_{Cu}, nm	h_{Cu}/h_W	τ_1, GPa	σ_{bond}, GPa	Grain Size, nm	Ψ, deg
181	0.165	1.27	5.23	110	12.7
505	0.459	1.45	5.34	130	15.2
1056	0.96	1.065	5.73	150	10.5
1930	1.75	0.663	5.13	180	7.4

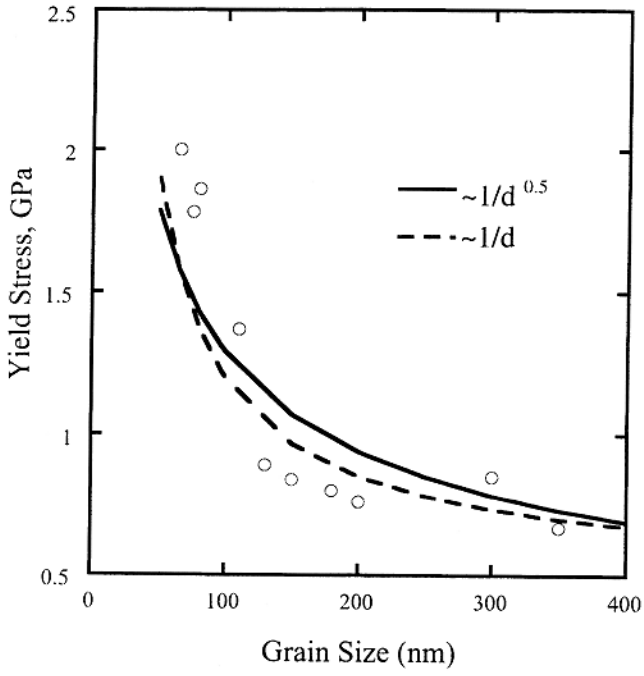

Fig. 10—Yield stress *vs* grain size. Solid line is the Hall–Petch relation.

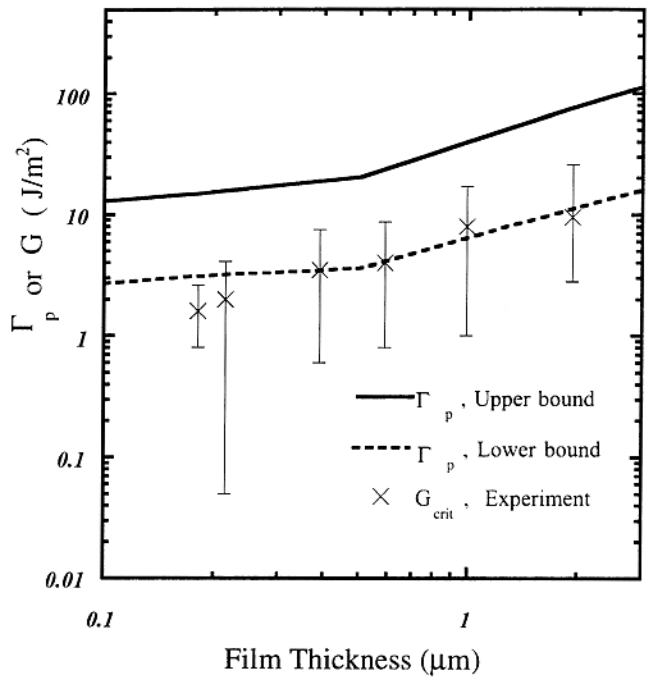

Fig. 11—An interfacial energy relationship to the film thickness: theoretical upper bound (solid line) and lower bound (dotted line) solutions as compared to experimental strain energy release rates. Note: error bars are full range of data, from 9 to 16 points.

been observed for several nanostructured materials, *e.g.*, Reference 28. However, even with the substrate effect correction, resulting yield stress values seem to be higher than would be expected for given grain sizes and film thicknesses. A possibility of an indentation size effect may not be excluded here. This necessitates a yield stress evaluation with alternative methods.

B. *Interfacial Energy Relationships to h_{Cu}*

The interfacial energy dependence on film thickness was found to be qualitatively similar for the experimental strain energy release rates and both upper and lower bound plastic energy dissipation calculations, as shown in Figure 11. For the film thicknesses lower than approximately 0.4 μm, the theoretical upper bound curve appeared to approach an asymptotic value of about 10 J/m^2. Unfortunately, significant scatter did not allow us to determine whether such a plateau existed for our experimental data. Such additional evaluation involving testing of a broader film thickness range is currently underway. However, regions with the measured work of adhesion independent of the film thickness were observed for different systems and testing methods[3,4] previously. It was concluded that plastic energy dissipation effects become significant only after some critical thickness. For the Cu/SiO_2 interface, this critical thickness was approximately 300 nm, which is in a good qualitative agreement with the value given by the upper bound solution.

Analysis of Eq. [9] shows that plastic energy dissipation is mainly determined by the product $h\sigma_{ys}^2$. For small film thicknesses, this value is almost constant because grain size scales with the film thickness yielding $\sigma_{ys}^2 \propto h^{-1}$. Note that this increase implies a Hall–Petch relation except that there is a fairly large σ_0 of 90 MPa. For the large film thicknesses, grain size increases at a much slower rate than film thickness and, consequently, plastic energy dissipation increases with the film thickness. It is possible that in the plateau region, plastic energy dissipation is independent of film thickness rather then being negligible as it was assumed earlier.[3,4]

While overestimating plastic dissipation effects slightly, the proposed upper bound model predicts the qualitative trends of the experimental results. One can also note that if the actual plastic zone is not through the Cu film, there is no reason for Eq. [9] to be in quantitative agreement. Better agreement may be expected for interfaces with higher interfacial fracture energy. On the other hand, a burgers vector as a cut-off distance should definitely be replaced by a more realistic measure such as the extent of the dislocation free zone. Finally, a possible overestimate in yield stress values would certainly contribute to an overestimate in plastic energy dissipation. Note that a lower bound solution seems to be in an excellent agreement with the experimental data, while an underestimate would be expected. This suggests an overestimate in R_p and/or yield stress values.

C. *Other Possible Sources of Elevated Toughness*

1. *Difference of the interface properties*

It may be argued that interface properties can vary with the film thickness. For example, longer sputtering times may lead to the elevation of the substrate temperature and, consequently, interface property changes. However, bond strength values given by Eq. [14] are almost independent on the film thickness, as shown in Table I Note that the magnitude of bond strength values seems reasonable as compared with values obtained for various metal/oxide interfaces.[29] First of all, bond strength values independent of film thickness implies that the interface property remains unaltered by longer sputtering times. Second, it suggests a

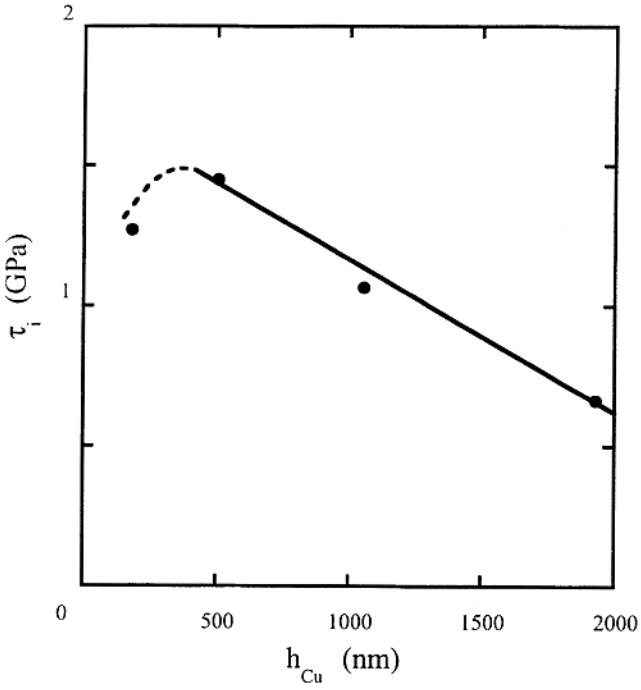

Fig. 12—Interfacial shear stress dependence on the relative Cu film thickness.

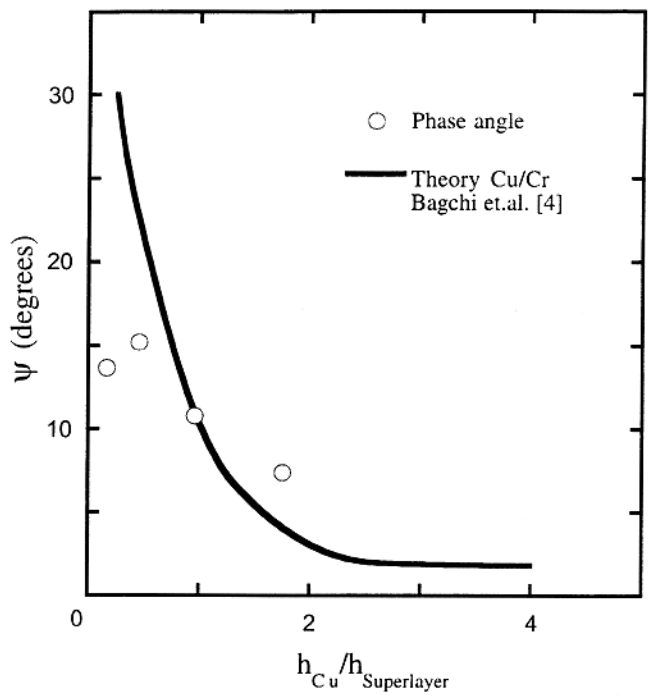

Fig. 13—Effects of the relative Cu film thickness on the mode mixity.

similarity of the phase angle for different film thicknesses. However, a more precise mode mixity evaluation is required.

2. *Mode mixity effects*

Interfacial shear stress estimated with Eq. [16] ranges from 600 to 1500 MPa, as shown in Figure 12. This is comparable with the results obtained by Dehm *et al.*[30] for the Cu/Al_2O_3 interface. In their research, shear stresses ranged from 400 to 1600 MPa for the similar film thickness range. The phase angle ψ determined with Eq. [17] is shown in Figure 13 alongside the theoretical values calculated for the same h_{Cu}/h_{Cr} ratios.[4] Despite the difference in the superlayer properties and a more complicated stress-strain state for our case, phase angle ranges are similar. The experimental values for Cu/W seem to drop with increasing $h_{Cu}/h_{superlayer}$ just as Bagchi and Evans predict for Cu/Cr. This is consistent with the qualitative predictions as detailed in the Appendix. It is necessary to emphasize that ψ changes only slightly and tends to drop with increasing Cu thickness. Since the toughness should drop (if anything) with a decreasing phase angle, an increased mode II component does not seem to be responsible for the increased toughness with the thicker Cu layers.

3. *Properties of the bilayer solution*

It may be suggested that the bilayer analysis used in the present research can give elevated toughness values for the higher film thicknesses due to the intrinsic properties of the solution. To evaluate such a possibility, calculated values of G were plotted *vs* a delamination radius/contact radius ratio for the 200 and 2000-nm-thick films, as shown in Figure 14. The bilayer solution can be represented as a family of curves, G *vs* *R/a*. Each curve corresponds to a pair of values of the film thickness and indentation depth. These lines are very closely spaced, and G values are determined mostly by *R/a* ratios. One of the lines for a 2000 nm film is shown in Figure 14. For comparison, theoretical curves for the single layer wedge indentation problem[10] are plotted for 2000- and 200-nm film thicknesses. Note that both solutions assume plane strain conditions. It is evident that for small *R/a*, G given by the bilayer solution increases very rapidly as *R/a* decreases. A similar trend is also observed for the wedge problem solution. The difference between G for 200 and 2000 nm film comes from the difference in the *R/a* ratio. Thus, trends in the interfacial fracture toughness are not likely to be produced just by solution artifacts.

Further analysis of Figure 14 raises other questions. For the measured G to be constant, the ratio *R/a* should be constant for a given thickness. However, it increases with the indentation depth/film thickness ratio as shown in Figure 15 for two different film thicknesses. Thus, crack propagation may be more difficult for small interfacial cracks. In this case, the crack tip state may be more affected by the stress-strain fields near the indenter tip. These effects to be addressed later will be referred to as "tip interaction effects." A consideration should also be given to possible crack tip plasticity effects. Prior to reaching quasistatic plastic zone conditions, plastic energy dissipation rates may be higher, thus, yielding higher interfacial toughness values for smaller cracks. Whatever the reason, it is clear that part of the large variation in Figure 14 and, hence, in Figure 11, is due to the steeply rising curves $G(R/a)$ and, perhaps, an inability to exactly determine delamination radii for such small interfacial cracks.

4. *"Tip interactions"*

Finite element solutions predict a maximum interfacial shear stress at approximately 0.8 and normal compressive stresses approaching zero at approximately 1.6 of the contact radius.[31] Thus, interfacial crack initiation is likely to occur at the edge of the contact area, which is consistent with *in situ* observations.[31] At the initial stage, the crack tip will

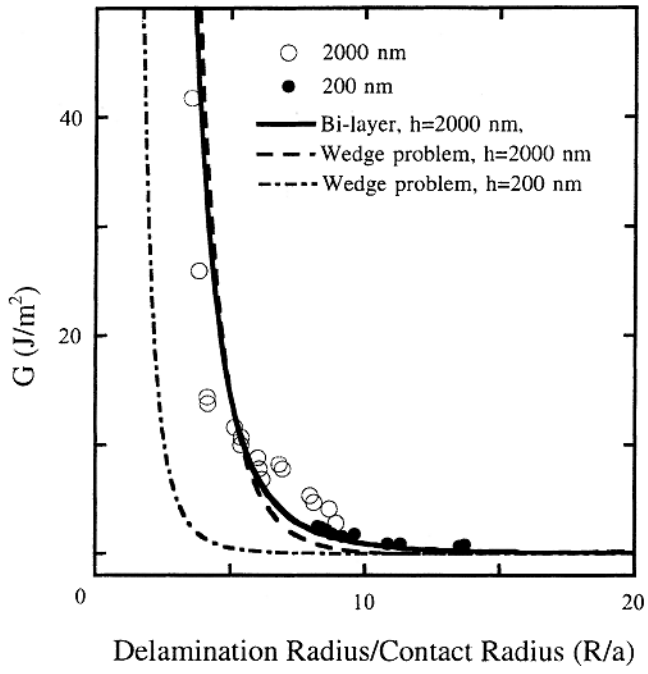

Fig. 14—Strain energy release rate as a function of the normalized delamination radius.

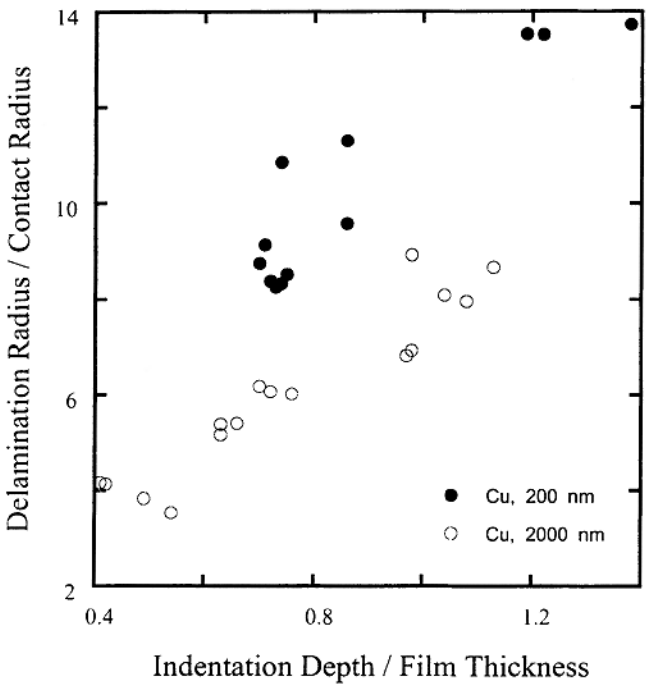

Fig. 15—Dependence of the normalized delamination radius on increasing penetration depth.

still be affected by compressive stresses. These compressive stresses may increase the effective shear strength of the interface by a Coulomb type dependence:[31]

$$\tau_c = \tau_{c0} + \mu\bar{\sigma}_z \qquad [18]$$

Here, τ_c is an effective interfacial shear strength; τ_{c0} is the intrinsic shear strength; μ is a frictional coefficient; and $\bar{\sigma}_z$ is the compressive stress. Increasing the effective shear strength may be one of the reasons for higher G values measured for indentations at smaller depths.

Thus, there could be different stages of the interfacial crack propagation depending on the relative depth/film thickness ratio. Also, unloading at different stages of the interfacial crack evolution will produce different conditions for the crack extension after the tip removal. In some cases, while strain energy is reduced due to buckling, change of the mode mixity due to buckling can reduce interfacial fracture toughness and, thus, make further crack advance possible. It follows that the determination of the time of final crack advance is of importance. Some insight can be gained with acoustic emission technique monitoring during a test and evaluation of interfacial fracture mechanisms by examining indentation induced blisters. With the previous method, some revisions/additions can be incorporated to account for the complexity of the processes occurring upon indentation induced interfacial crack propagation.

V. SUMMARY AND CONCLUSIONS

A theoretical model has been proposed for the plastic energy dissipation effects on the interfacial fracture toughness. The model predictions were compared to experimental results obtained from indentation tests using the axysymmetric bilayer theory. Comparison involved RF sputtered Cu thin film interlayers between oxidized silicon and sputtered tungsten. Experimental values for the Cu/SiO_2 interface ranging from 2 to 10 J/m^2 increased with the film thickness in qualitative agreement with the theoretical predictions. A proposed method for bond strength evaluation allowed determination of a bond strength of approximately 5 to 6 GPa relatively independent of the film thickness. Phase angle calculations yield phase angles decreasing with film thickness. Consequently, the observed interfacial toughness increase cannot be attributed to either mode mixity effects or increasing intrinsic interfacial fracture energies. Taking this into account, plastic energy dissipation has been identified as the mechanism responsible for the observed elevation of the interfacial fracture toughness.

Analysis of the experimental data suggests the existence of different stages of interfacial crack propagation as might be influenced by tip interaction stresses and plastic zone evolution. The present bi-layer analysis needs to be modified to account for these processes for more precise measures of interfacial fracture toughness.

ACKNOWLEDGMENTS

The authors acknowledge support for this work by the Center for Interfacial Engineering, University of Minnesota, under Grant, No. NSF/CDR-8721551; and the Department of Energy, under DOE Contract No. DE-FG02/96ER45574. In addition, NIT thanks Professors J.V.R. Heberlein and S.L. Girshick, University of Minnesota, for support under NSF DMI-9871863. The assistance of Dr. J.C. Nelson, Center for Interfacial Engineering, and Microtechnology Laboratory staff, University of Minnesota, is also gratefully appreciated.

APPENDIX

Effects of film thickness and interfacial crack length on the mode mixity for buckling driven delamination in the

indented prestressed film can be qualitatively evaluated through the parameter $\eta = \sigma/\sigma_c$. Here, σ_c is the critical buckling stress; $\sigma = \sigma_i + \sigma_R$ is the total stress in the film; and the σ_i and σ_R are the indentation induced stress and residual film stress, respectively. As η increases, $|\psi|$ increases with the interface crack becoming more heavily under mode II conditions.[19] The parameter η can be determined using values of σ_i and σ_R defined by Marshall and Evans's[11] analysis for a single layer, giving

$$\eta = \frac{\sigma_i + \sigma_R}{\sigma_c} = \frac{\sigma_R + \beta E V_0/R^2 h}{\gamma E h^2/R^2} = \frac{\sigma_R R^2 + \beta E V_0/h}{\gamma E h^2} \qquad [A1]$$

Here, $\gamma = 14.68/12(1 - \nu^2)$; $\beta = 1/2\pi(1 - \nu)$; V_0 is the indentation volume; ν is Poisson's ratio; E is Young's modulus; and compression is regarded as a positive stress. In the case of a bilayer film, σ_R should be replaced with the *effective* residual stress in the laminate. For the Cu/W thickness ratios and residual stress levels considered in the present research, the effective σ_R is always positive.

Differentiating Eq. [A1] with respect to the delamination radius yields

$$\frac{\partial \eta}{\partial R} = \frac{2\sigma_r R}{\gamma E h^2} \qquad [A2]$$

As follows from Eq. [A2], η increases with the delamination radius if the effective residual stress in the bilayer is compressive.

On the other hand, the derivative $\partial\eta/\partial h$ is always negative, providing $\sigma_R > 0$:

$$\frac{\partial \eta}{\partial h} = -\frac{1}{E\gamma}(2\sigma_R R^2/h^3 + 3\beta E V_0/h^4) \qquad [A3]$$

Thus, mode mixity decreases with increasing film thickness, which is consistent with the experimental calculations.

REFERENCES

1. A. Furua, N. Hosoi, and Y. Oshita: *J. Appl. Phys.* 1995, vol. 78, pp. 5989-92.
2. R.G. Stringfellow and L.B. Freund: *Int. J. Solids Struct.*, 1993, vol. 30, pp. 1379-95.
3. S. Venkataraman, D.L. Kohlstedt, and W.W. Gerberich: *J. Mater. Res*, 1996, vol. 11 pp. 3133-45.
4. A. Bagchi and A.G. Evans: *Thin Solid Films*, 1986, vol. 286, pp. 203-12.
5. Z. Sou and J.W. Hutchinson: *Int. J. Fract.*, 1990, vol. 43, pp. 1-18.
6. K. Bose, P.A. Mataga, and P. Ponte Castaneda: *Intern. J. Sol. & Struct.*, 1999, vol. 36, pp. 1-34.
7. H. Gleiter: *Nanostruct. Mater.*, 1999, vol. 6. pp. 3-14.
8. G.W. Nieman, J.R. Weertman, and R.W. Siegel: *J. Mater. Res.*, 1991, vol. 6, pp. 1012-27.
9. M.D. Drory and J.W. Hutchinson: *Proc. R. Soc. London A*, 1996, vol. 452, pp. 2319-41.
10. J. Vlassak and W.D. Nix: *J. Mech. Phys. Solids*, 1996, vol. 42, pp. 1223-45.
11. D.B. Marshall and A.G. Evans: *J. Appl. Phys.*, 1984, vol. 56, pp. 2632-38.
12. M.Y. He, A.G. Evans, and J.W. Hutchinson: *Acta Metall. Mater.*, 1996, vol. 44, pp. 2963-71.
13. M.D. Kriese, N.R. Moody, and W.W. Gerberich: *Acta Mater.*, 1998, vol. 46, pp. 6623-30.
14. M.D. Kriese, N.R. Moody, and W.W. Gerberich: *J. Mater. Res.*, 1999, vol. 14, pp. 3007-18.
15. M.D. Kriese, N.R. Moody, and W.W. Gerberich: *J. Mater. Res.*, 1999, vol. 14, pp. 3019-25.
16. F.A. McClintock: *J. Appl. Mech.*, 1958, vol. 25, pp. 582-88.
17. F.A. McClintock and G.R. Irwin: *Plasticity Aspects of Fracture Mechanics, Fracture Toughness Testing and Its Applications*, ASTM STP 381, ASTM, Philadelphia, PA, 1965, pp. 84-113.
18. J.R. Rice: *Fatigue Crack Propagation*, ASTM STP 415, ASTM, Philadelphia, PA, 1967, pp. 247-309.
19. J.W. Hutchinson, M.D. Thouless, and E.G. Linger: *Acta Metall. Mater.*, ASTM, 1992, vol. 40, pp. 295-308.
20. S.X. Mao and A.G. Evans: *Acta Mater.*, 1997, vol. 45, pp. 4263-69.
21. K.J. Hsia, Z. Sou, and W. Yang: *J. Mech. Phys. Solids*, 1994, vol. 42, pp. 877-96.
22. W.W. Gerberich: University of Minnesota, Minneapolis, MN, unpublished research, 1998.
23. D. Tabor: *The Hardness of Metals*, Claredon Press, United Kingdom, 1951, pp. 174.
24. W.W. Gerberich, J.C. Nelson, E.T. Lilleodden, P. Anderson, and J.T. Wyrobek: *Acta Metall. Mater.*, 1996, vol. 44, pp. 3585-98.
25. T.W. Wu: *J. Mater. Res.*, 1991, vol. 6, pp. 407-26.
26. W.C. Oliver and G.M. Pharr: *J. Mater. Res.*, 1992, vol. 7, pp. 1564-83.
27. A. K. Bhattacharya and W.D. Nix: *Int. J. Solid Struct.*, 1988, vol. 24, pp. 1287-98.
28. J.B. Savader, M.R. Scanlon, R.C. Cammarata, D.T. Smith, and C. Hayzelden: *Scripta Mater.*, 1997, pp. 29-34.
29. J.R. Smith, T. Hong, and D. Srolovitz: *Phys. Rev. Lett.*, 1994, vol. 72, p. 4021.
30. G. Dehm, M. Ruhle, H.D. Conway, and R. Raj: *Acta Mater.*, 1997, vol. 45, pp. 489-99.
31. J.E. Ritter, T.J. Lardner, Rosenfeld, and M.R. Lin: *J. Appl. Phys.*, 1989, vol. 66, pp. 3627-34.